

Citation for published version:

H. Zhang, H. Yang, H. J. Chen, X. Du, D. Wen, and H. Wu,
'Photothermal conversion characteristics of gold nanoparticles
under different filter conditions', *Energy*, Vol. 141: 32-39, September
2017.

DOI:

<https://doi.org/10.1016/j.energy.2017.09.059>

Document Version:

This is the Accepted Manuscript version.

The version in the University of Hertfordshire Research Archive may
differ from the final published version.

Copyright and Reuse:

© 2017 Elsevier.

This manuscript version is distributed under the terms of the
Creative Commons Attribution-NonCommercial-NoDerivatives
License CC-BY-NC-ND (<http://creativecommons.org/licenses/by-nc-nd/4.0/>), which permits non-commercial re-use, distribution, and
reproduction in any medium, provided the original work is properly
cited, and is not altered, transformed, or built upon in any way.

Enquiries

If you believe this document infringes copyright, please contact the
Research & Scholarly Communications Team at rsc@herts.ac.uk

Photothermal conversion characteristics of gold nanoparticles under different filter conditions

H. Zhang^a, H. Yang^a, H.J. Chen^b, X. Du^a, D. Wen^c, H. Wu^{d,*}

^a *Laboratory of Condition Monitoring and Control for Power Plant Equipment of Ministry of Education, School of Energy and Power, North China Electric Power University, China*

^b *State Key Laboratory of Optoelectronic Materials and Technologies, School of Electronics and Information Technology, Sun Yat-Sen University, Guangzhou, China*

^c *School of Process, Environmental and Materials Engineering, University of Leeds, United Kingdom*

^d *School of Engineering and Technology, University of Hertfordshire, Hatfield, AL10 9AB, United Kingdom*

*Corresponding author. Email: h.wu6@herts.ac.uk Tel. +44(0) 1707 284265;
Fax. +44(0) 1707 285086

Abstract

In this article, plasmonic nanoparticles (PNP) were used to improve the solar thermal conversion efficiency and the abortion prosperity under eight different wavelength spectrum was compared. Gold nanoparticles (GNP) is synthesized through an improved citrate-reduction method, which was used to illustrate the photo-thermal conversion of PNPs under a solar simulator with eight filters. Experimental results showed that the best light intensities at wavelength of 710 nm could reach 0.004 W/cm² when applied to two suns. With the increase of the irradiation time, the GNP temperature increased linearly and the temperature could be increased by 3.5 K within 300 s. In addition, there were no infrared, no visible light, and no UV filters utilized to compare GNP photothermal conversion efficiencies in three main spectrum regions. As eight filters were applied in the current experiment, more specified wavelength spectrum and longer time need to be tested for the purpose of optimisation.

Keywords: plasmonic nanoparticles, wavelength spectrum, photo-thermal conversion efficiency, light filter.

Nomenclature

		Greek
A	area (m^2)	ϵ extinction coefficient
c	specific heat ($\text{J/kg}\cdot\text{K}$)	ϕ volume fraction(%)
d	particle diameter (m)	η photothermal conversion efficiency
I	solar intensity (W/m^2)	Δ difference
L	distance of light travelled (m)	
m	mass (kg)	Subscript
p	Radiation transmitted through a sample (W/m^2)	
P_0	Incident radiation (W/m^2)	n nanoparticle
SAR	specific absorption (W/g)	w water
T	Temperature (K)	UV Ultraviolet Rays
t	time (s)	VIS visible
		IR Infrared Spectroscopy

1. Introduction

Nowadays it can be recognized that nanomaterials could produce completely different characteristics from the traditional material in terms of surface effect, small size effect, quantum size effect and other physical and chemical properties. Nanomaterials has been widely applied in the fields of energy, chemicals, automotive, construction, microelectronics and information. Nanotechnology has become a hot topic in the nanomedicine, nanochemistry, nanoelectronics, nanomaterials, nanobiology and other public areas.

Nanofluids (NNFs), as part of the nanomaterials, which attracts wide range applications in practical. Combining photovoltaic with solar thermal utilization such as solar heat and power plant, it can improve the utilization of the solar radiation, reducing the operating temperature of the battery pack. Thus, the power generation efficiency can be improved tremendously. In the solar power plants, due to the heat transfer medium working at a temperature range of 300-700 °C, nanofluids properties of the metal will be impacted accordingly. What's more, the nanoparticles will be precipitated and accumulated. Accordingly, further research is needed for solar power applications.

Kim et al. [1] applied thermal energy balance to analyze the thermal performance of a U-tube solar collector using 20% PG (propylene glycol) as the working fluid. In

their study, solar collector efficiency was calculated and energy savings was predicted for various nanofluids, such as MWCNT, CuO, Al₂O₃, SiO₂ and TiO₂. It was found that the solar collector efficiency increased in the following order from greatest to least: MWCNT, CuO, Al₂O₃, TiO₂, and SiO₂ nanofluids. Kim et al. [2] experimentally investigated the efficiency of a U-tube solar collector as a function of the concentration of Al₂O₃ nanofluid and the size of the nanoparticles. It was concluded that the Al₂O₃ nanofluid was effective in increasing the efficiency of the U-tube solar collector. In the research work of Al-Nimr and Al-Dafaie [3], a mathematical model was developed to test the transient temperature distribution of the silver nanofluid pond at different volume fractions, heat transfer coefficients and exposure time conditions. Comparing with conventional solar pond and conquered the traditional brine ponds troubles, presented nanopaticles had obvious advantages in solar storage. Chen et al. [4], Kosuga et al. [5], Lenert and Wang [6] and De Boni et al. [7] set up test rigs to investigate the absorption of the gold or silver nanoparticles at different specialized wavelength range of 500-1000 nm. All their experimental results showed that the temperature increased remarkably and the efficiency was analyzed as a direct absorption solar collector.

The working medium in the solar energy systems play an important role in solar absorption. Colangelo et al. [8] investigated the Al₂O₃-therminol nanofluids property, such as stability, viscosity, FI-IR spectra, cluster size and thermal conductivity. It would be very helpful to evaluate the non-Newton fluid characteristic in the solar absorption system. Over the past decades, many researchers devoted to study the nanofluids photothermal absorption characteristics. It is recognized that the rate of the absorption was influenced by nanopaticles length, diameter, volume fraction and particle size distributions [9-12]. Mercatelli et al. [13], Chen et al. [14] and Karami et al. [15] investigated TiO₂, Al, Au, SiO₂, silver, copper-oxide and carbon nanotubes at corresponding optimal heat absorption wavelength of light itself with particle sizes, concentrations, lengths, and diameter. It was found that there is a great difference in the optimum wavelength, that is, with the growth of the nanorod diameter and length, the optimal wavelength increases. Lucas et al. [16] conducted an experimental study to

investigate the grand optical absorption at wavelength of 808 nm. It was observed that when the light intensity was increased, the surface of the nanopartical temperature was linear. It was stated that the combined micro-electromechanical systems (MEMS) with the infrared absorbent gold nanoparticals have significant potential application in light-actuated switches and mechanical construction. Kim et al. [17] concluded that taking advantage of nanofluid photothermal prosperity in catalyst would also have a positive effect. Nair [18] performed an experiment to study the 20-30 nm Ag/TiV oxide grain samples in UV-DRS spectra. Their result showed that in the visible light photocatalytic activity of Ag/TiV oxide better three and seven times than TiV oxide and Degussa P25 respectively. Due to different working materials, the line of the absorption TiV/Ag oxide and Degussa P25 decreased abruptly at around 390 nm in UV-DRS spectrum.

In recent years, the application of nanofluid in medical engineering has obtained great achievements. El-Sayed et al. [19] and Ou et al. [20] found that the malignant cells require no more than half of the power energy leading to benign cells nobinary. With anti-EGFR/Au conjugates bonded easily and it has a high efficient absorption near the visible spectrum band. Taking advantage of precious metal heat transfer characteristics, experimental medium is gold nanoparticles in genaral. For example, in the application of killing cancer cells, Ye et al. [21] used nanotubes as the core of the body to stimulate the outsourcing of the organic matter, in particular of the laser wavelength action. The cancer cells would be heated up to 42°C, then it will be dying. Experimental results showed that the survival rate of the cancer cells significantly decreased. When do experiments on mouse body, equipments can detect concentrations of the different parts of the gold nanotubes in the organs. The 700-900 nm nanoparticles carry drugs as targeted heat by the laser to kill the cancer cells. Liu et al. [22], Bhana et al. [23], Zhou et al. [24] and Paci et al. [25] performed fundamental research on the goldnanoparticles that used in drug manufacturing. In the near-infrared wavelength, gold nanoparticles showed good light absorption properties.

Ebrahimian and Ansarifar [26] studied the nanofluid performance in VVER-1000 nuclear reactor core. Due to the excellent heat transfer coefficient of the nanofluid, it

would be an ideal method for cooling annular fuel. With smaller nanoparticle size and bigger volume fraction, the temperature of the fuel center decrease. In addition, it was found that 0.03 volume fraction and 10 nm size of Al_2O_3 achieved the best presentation in regular circulation. Garoosi et al. [27] conducted a numerical study to examine two dimensional containing circular cylinder correlation parameters: Rayleigh number, volume fraction, particle size, type of nanomaterial, shape of the enclosure and the orientation of the hot and cold cylinders etc. However, after Lee and Kang [28] used aqueous solution nanofluids to enhance the CO_2 absorption of the base fluid, it is concluded that the effect of the nanoparticles on the mass transfer enhancement is more significant in the region of unsaturated state than that of the saturated state.

Mercatelli's results revealed that 270 nm wavelength absorption up to maximum while at the lowest penetration rate and with the volume increase penetration rate show a downward trend [13]. Although in a low concentration of GNPs based on the fluid i.e. 0.15 ppm, the solution has great performance in photothermal absorption efficiency. In the near-infrared wavelength absorption rate to can be creep to 12°C within 300 s. Gold nanofluid characteristic with a different circumstance showed different performance in photothermal absorption and radiation [29-30]. Kosuga took advantage of photothermal films in assembling particular energy of the solar spectrum, temperature rise up to 40 °C only in 100 s [5].

It is aforementioned from the above research works, gold nanofluid has huge perspective in the near future that can be used in heat convention and solar absorption domain. However, previous studies have shown that the extinction coefficient do not represent the real photo-thermal energy conversion process, especially for the photothermal conversion experiment in the whole spectrum. Therefore, it has still much room to investigate the photothermal conversion performance of the GNPs in a single wavelength. The objective of the current work is to use five slices filters to study the photothermal conversion performance of GNPs by measuring temperature changes of the fluid in a single wavelength. In the current study, five different filters will be used to investigate the photothermal conversion performance of the GNPs and

the temperature of the nanofluid changes will be measured in a single wavelength comparing with other related research results.

2. Experimental approach

2.1. Gold nanoparticle synthesis and characterization

In general, gold nanoparticles can be synthesized by three methods: citrate reduction (CR) method, the Brust-Schiffrin method, and the modified Brust-Schiffrin method. In the present work, we will take citrate reduction method which is similar to Chen and Wen [31], Philip [32] and Kim [33]'s preparation of goldnanoparticle aggregates with three different methods. The base solution is HAuCl₄ in potassium carbonate (K₂CO₃) solution (K-gold solution) and then adding (a) L-ascorbic acid, (b) alcoholic solvents, (c) NaBH₄ respectively. During the experiment, all of the solutions were exposed in the wavelength range of 300 to 1100 nm using Agilent UV-Visible spectrometer. The result shows that the extinction curves have a peak value of weave occurs at around 700 nm.

During the experiment, gold nanoparticles dispersions are formulated through simultaneous production and dispersion of the nanoparticles *in situ*. GNPs were synthesized by the citrate reduction method with the aid of ultrasonication for particle morphology control [34]. According to CR method, 5.0×10^{-6} mol of HAuCl₄ was added to 190 ml (DI) water and mixed solution was heated until boiling under the magnetic blend condition. 10 ml of sodium citrate (0.5%) was added to the HAuCl₄ solution, then, the solutions were placed in the 80°C ultrasonic bath for 30 min until its color changed to wine-red. GNP dispersions were purified by the membrane dialysis method.

In the current experiment, 100 ml of GNP dispersion was added to the membrane tube with 2-3 nm in diameter, which allows the diffusion of the ions but keeps GNPs at it. Then, the membrane was put in a flask of DI water, stirred by a magnetic blender. The DI water was replaced twice per day and this step lasted for five days. Based on the UV-Vis spectrum test results, the concentration of various impurities diminished exponentially with the increasing DI water changing times. In the current work, the

photothermal conversion effect can be ignored. The gold nanoparticles mass concentration is 0.0028% (1.5 ppm).

The concentration of the gold nanoparticles solution is measured by an atomic absorption spectrometer (Varian 220FS SpectrAA Atomic Absorption Spectrometer & GTA110) transmission electron microscopy (TEM) equipped with an Energy Dispersive X-ray spectroscopy (EDX) was applied to identify the size and shape of the nanoparticles and take 200 KV as its bias voltage. Dynamic light scattering (DLS) device (Malvern nanosizer) was used to observe the particle size distribution in the solution. As shown in Fig. 1, the gold nanoparticles presents in clear red-wine color and in the ball shape according to the TEM images. In Fig. 2, almost 90% of GNPs diameters in the range of 15 nm to 30 nm in the DI water. Apparently, TEM measurement is a bit smaller than the DLS values. GNPs dispersion status in the solution on the basis of the DLS results is illustrated in Fig. 2.

2.2. Photothermal conversion experiment

Photothermal conversion experimental equipment was schematically shown in Fig. 3. For the case of producing big deviation in the sunlight directly, a solar simulator (Newport Co. Oriel Xenon Arc lamp) was applied to simulate the light source. This could generate spectral as similar as solar and it can change the radiation intensity in between 1 am and 2 am. The test facility can be well performed according to the ASTM standard (ASTM G-173, 2011), such as temporal instability below 5%, non-uniformity of irradiance of up to 5% and spectral match (fraction of ideal percentage) of 0.7-1.25. In order to minimize the deviation due to the temperature gradient, GNPs dispersion was spread in the dish no more than 3 mm and was covered with a glass sheet (3.5 cm diameter), which was put in the solar simulator central spot. There are different filters below the sunlight producer which light could through length, including 410, 520, 710, 860, 1064 nm. Light through the filter which concluding visible spectrum 410, 520, 710 nm and infrared wavelength 860, 1064 nm heat gold nanofluid. K-type thermocouple (Omega 5TC-TT-K-36-36) was used to measure the sample temperature located at the bottom center of the Petri dish. In the labview environment, achieved date was deposited in a PC though a data acquisition

hardware (thermocouple input devices, NI, USB-9211, 4-Channel, 24-bit).

3. Results and discussion

Prior to the discussion, it is worthy to mention air mass (AM) which is normally used in the photothermal conversion experiments, and it represents the solar spectrum at mid-latitudes. According to the standard of ASTM G-173, the solar intensity (I) is 1000 W/m^2 at $\text{AM}=1.5$. Solar radiation energy concentrated between 150-4000 nm wavelength. During this wavelength range it can be divided into three main regions, i.e., shorter wavelength ultraviolet, longer wavelength infrared regions and visible regions. Solar radiation energy mainly accumulates in the visible and infrared regions, the former accounting for 50% of the total amount of solar radiation, while another accounted for 43%, only 7% in the ultraviolet regions. In the vicinity of 475 nm wavelength, solar radiation power reaches the highest value. It is found that in the near-infrared (NIR) region it shows significantly photothermal absorption property and it could be used for controlling as the external stimulus to motivate drug release [35]. In the present study, solar simulator can emit similar to the sunlight wavelength light intensity, and with filters which only five light wavelengths could through it. Its spectral irradiance can be clearly shown in Fig 4.

Since the Earth is an elliptical orbit around the Sun, the distance between the Sun and the Earth is not a constant. The average distance is $1.5 \times 10^8 \text{ km}$, therefore, the Earth's atmosphere solar radiation intensity is almost a constant. It is called "solar constant" which can be used to describe the intensity of the solar radiation above the Earth's atmosphere. It refers to the solar radiation that at the average Earth-Sun distance and beyond the Earth's atmosphere bound, per unit surface area perpendicular received. After the detection, international academic community agrees that "solar constant" is taken to be 1357 W/m^2 . During the current experiment, using 1 Sun, at 710 nm the intensity can reach 1500 W/m^2 , but only reach maximum 3500 W/m^2 in the two Sun power. When the "solar constant" more than twice of the original value, each specific wavelength of the light intensity has increased, but not to multiply increased. At 710 nm, the light intensities is increased to $2.10 \times 10^{-3} \text{ W/m}^2$,

while increased to 1.55×10^{-3} W/m² at 520 nm. However, at 710 nm, the light intensities increments are four times that at 860 nm. At 410 nm and 1064 nm, almost no influence on the light intensity when add the "solar constant". It can be observed that increasing the "solar constant" the light intensities could be changed at different wavelengths.

Fig. 4 shows the variation of the spectral irradiance with wavelength. The solar radiation spectrum at five different filters, i.e., 410, 520, 710, 860 and 1064 nm are illustrated. It can be obviously observed that the spectral irradiance in the visible wavelength is higher than that in the infrared wavelength. However, as illustrated in Fig. 5, near the infrared wavelengths, the photothermal conversion efficiency performs better than that at visible light wavelength. Ye et al. [21] explored different lengths goldnanotubes absorption properties and similar results was obtained. Zhou et al. [24] found the advantage of the gold nanoparticles which have a high photothermal conversion efficiency near infrared region, raising the cancer cell temperature up to 42 °C. In their experiment, DI water and nanofluids were light 300 s, the highest temperature appeared in the near infrared region. At 1064 nm, the nanofluid temperature raising 3.4°C, DI water temperature is increased only by 2.5°C. At five different wavelengths, the largest slope occurs at 1064 nm, that is, with longer exposure time, the temperature will continue to increase. Nanofluid temperature is increased about 3.5 °C at 710/860 nm, but water absorption is lower.

Gold nanopartical temperature can be taken as solution temperature, which can be measured by thermocouple at the bottom of the dish. On the other hand, nanofluid temperature can be assumed as uniform since the depth of the solution is no more than 3 mm.

The photothermal conversion efficiency (η) can be formulated by [29]:

$$\eta = \frac{(c_w m_w + c_n m_n) \Delta T}{I A \Delta t} \quad (1)$$

where c_w , c_n are the specific heat of the water and nanoparticle, respectively. m_w , m_n are the mass of the water and nanoparticle, ΔT stands for the whole temperature rise in a Δt time interval. A represents the illumination area of the fluid in the experiment.

Since the particle concentration can be ignored ($\frac{c_n m_n}{c_w m_w} \sim 0$), the photothermal conversion efficiency can be rewritten as:

$$\eta \approx \frac{c_w m_w}{IA} \cdot \frac{\Delta T}{\Delta t} \quad (2)$$

Clearly the efficiency is directly linear to the temperature rise rate.

As shown in Fig. 6, the efficiency curve is opening upward parabola. From 410 nm to 520 nm, compared with DI water and GNPs, the η did not significantly increase. In addition, with the increase of the wavelength the efficiency curve turns to a downward trend. When the wavelengths are more than 710 nm, the efficiency increases linearly, at 860 nm it increased by about 5%, and reached a maximum 20% at 1064 nm. Compared with that in Fig. 6, between 710 nm and 1064 nm, the light intensity is decreasing, whereas the efficiency shows in the opposite direction. It has been obviously demonstrated that there is no relationship between the light intensity with the absorption efficiency and photothermal absorption efficiency. Their performance depends on the nature properties of itself.

It is defined that the ratio of the radiant power transmitted (P) divided by the radiant power incident (P_0) as the transmittance of the sample i.e. P/P_0 , which reveals the absorption spectrum. It was measured by a spectrometer (PerkinElmer, lambda 35) of nanogold spitting at various concentrations. Based on the Beer's law, the absorbance can be formulated as the logarithm (base10) of the reciprocal of the transmittance [29], as shown:

$$\log\left(\frac{P_0}{P}\right) = \varepsilon \phi L \quad (3)$$

where ε is the extinction coefficient, ϕ represents the volume fraction, L stands for the length of the light passing through the nanofluids. Since ϕL could be regarded as a constant value, the former formulation can be simplified to $\log\left(\frac{P_0}{P}\right) \propto \varepsilon$. Fig.7 can reflect the extinction coefficient changes directly.

Fig. 7 illustrates the variation of the gold nanoparticle mass

concentrations. It shows that similar tendency is obtained in the current study. The absorbance spectrum decreases initially with the wavelength range of 300-460 nm, followed a peak value at around 520 nm and then continue tending to decrease till the end. For the case of same wavelength, the higher the mass concentrations the larger the extinction coefficient, but the increment of the absorption efficiency decreases with double mass concentrations. There must exist an optimum value between the increment of the mass concentrations and the extinction coefficient. Compared with the results shown in Fig. 5, within the infrared wavelength region, photothermal conversion is well performed while the extinction coefficient is very low. By contrast to that in Fig. 4, at the vicinity of 710-1064 nm, the light intensity is very good, but the extinction coefficient is almost down to zero. Based on the above analysis, not obvious link between the light intensity and the extinction coefficient is observed. It somehow depends on the nature of the nanoparticles.

Fig. 8 demonstrates the temperature profiles when the solar simulator combined with the UV-VIS, UV-IR and VIS-IR waveband spectrum filters radiate under two cases of DI water and GNPs 300 s. For the case of the VIS-IR exposure GNPs the temperature can reach 10 °C, and the DI water temperature rise is very close to 7.5 °C. In the UV-IR region, the goldnanoparticles temperature increased by only 4 °C, whereas the DI water temperature is almost unchanged. GNPs temperature slope is only 4/300 while the case for the DI water is less than 2/300. Markedly different irradiated with UV-IR, VIS-IR spectrum could be up to 10/300 for twofold former cases. In this figure, the UV-VIS, VIS-IR, DI water temperature can increase about 6 °C, it proved that most of the energy of the sun concentrated in the vicinity of the visible spectrum. For GNPs, at VIS-IR spectrum, it contributes to a higher thermal efficiency and UV-VIS afterwards. It can also be noted that the temperature slope shows a decreasing trend after 300 s, i.e. exposed continuous light, GNPs temperature would be verge to a stable value exposed light in a long time.

The particle's capability in absorbing energy per unit mass can be described as the specific absorption rate (SAR), as shown in Fig. 9. According to [34], the lowest particle concentration leads to the maximum SAR.

SAR can be calculated as [29]:

$$SAR = \frac{(C_w m_w + C_n m_n) \Delta T_N - C_w m_w \Delta T_w}{1000 \cdot m_n \Delta t}, [kW/g] \quad (4)$$

where ΔT_N and ΔT_w are the temperature increments at the same Δt time interval for water and nanofluids respectively. Apparently, $\frac{C_w \Delta T_N}{1000 \Delta t} \approx 0$, then, the SAR calculation can be simplified as:

$$SAR = \frac{C_w m_w}{1000 \cdot m_n} \left(\frac{\Delta T_N}{\Delta t} - \frac{\Delta T_w}{\Delta t} \right) \quad (5)$$

And $\frac{C_w m_w}{1000 \cdot m_n} \left(\frac{\Delta T_N - \Delta T_w}{\Delta t} \right) = CONS$, so $SAR \propto (\Delta T_N - \Delta T_w)$, i.e. SAR valuation is lie on the difference of the temperature rise between the nanoparticle dispersion and the base fluid.

In Fig. 9, within the VIS-IR region, the SAR can reach to the maximum value of 2kW/g, which is higher than the other two cases, i.e., UV-VIS and UV-IR. When the visible wavelength content reduces, the SAR value decreases accordingly. As illustrated in Fig. 5, the maximum temperature difference of GNPs and water is at 710 nm-1064 nm, while the minimum temperature difference occurs at 410 nm. This coincides with the present experimental data that the lowest photothermal efficiency appeared in the vicinity of the ultraviolet light. It can be recognized that the optimal photothermal conversion efficiency could be within the visible light region. In a previous study, Zhang et al. [29] studied the relationships between the SAR and the GNPs concentration changes in the whole wavelength ranges, whereas the current work is to investigate the relationship between the SAR and the other two wavelength regions of allareasa. Apparently, it is essential to study the relationship between SAR and GNPs mass concentration within a certain wavelength region [29].

Fig. 10 shows the comparision of the photothermal conversion efficiency between the GNPs and DI water in UV-VIS, UV-IR and VIS-IR waveband. Exposed at different wavelength regions, as demonstrated in Fig. 10, the optimal photothermal

conversion efficiency (η) of the gold nanoparticle could reach 30% in VIS-IR waveband instead of 20% in a single wavelength 1064 nm only 20% that shown in Fig. 5. It is beyond imagination that η of the DI water attain 20% in VIS-IR waveband is equal to 1064 nm. And the difference value of η between GNPs with DI water is 10%, while the most differentials only 5% in 860 nm, as shown in Fig. 5. Compared with the results in Fig. 9, the photothermal conversion efficiency is similar to the SAR histogram trend in the corresponding area for UV-VIS/UV-IR/VIS-IR. In UV-VIS/VIS-IR wavebands, both of them contain visible wavelength regions, when the temperature increases, SAR and η shows better presentations. In He's report [36], the transmittance of the Cu-H₂O nanofluids over solar spectrum (250-2500 nm) was invested by UV-Vis-NIR spectrophotometer according to the integrating sphere principle. For the lights in Fig. 6, the transmittance of the Cu-H₂O nanofluids are down to zero near infrared spectra range of 1370-2500 nm yet has excellent transmittance in the 500-1370 nm. It was concluded that the absorption coefficient of the Cu-H₂O nanofluids presents the best performance in the UV waveband then sliding smoothly with the wavelength increasing in the visible area, and then rise abruptly in the infrared. By comparison with the experiment of [36], the result is totally different what have achieved from the current work. Considering the results from Figs. 9 and 10, the photothermal conversion efficiency (η) of the GNPs VIS waveband has better absorption coefficient than that for UV and IR. Recently, Jin et al. [37] performed a combined experimental and numerical stduy to investigate the photothermal conversion efficiency of the gold nanofluid under natural solar irradiation condition. In their study, when the visible light range from 500 nm to 800 nm mainly contribute to the absorption which achieves good agreement. Based on the comparative analysis, different nanofluid material can reach high photothermal conversion efficiency in a specified condition in terms of goldnanoparticle. It can be recognized that the nanofluid material could have the potential to absorb the solar radiation in the VIS-IR light range.

4. Conclusions

This work experimentally investigates the photothermal conversion characteristics at a single wavelength and waveband of sunlight emitted by solar simulators of gold nanoparticle dispersion. Major findings based on the experimental results are as follows::

- (1) There are no direct relationships between the light intensities, extinction coefficient and photothermal conversion, whch depends on the prosperities of the nanoparticles itself.
- (2) GNPs achieves the best photothermal conversion efficiencies at 710-1064 nm infrared waveband. Both the visible light and infrared waveband shows better temperature rise than that in a single wavelength region.
- (3) Photothermal conversion efficiencies of the GNPs under different filter conditions show remarkable performance i.e. 20% enhancement in vicinity of 1064 nm.
- (4) Two thirds of the waveband fields through GNPs show prodigious results that VIS-IR has the best photothermal absorption than the other two regions indicated by temperature increment and slope.
- (5) Both SAR and η show better presentations in VIS-IR wave region, and η does have been improved compared with that without GNPs.

Acknowledgements

This study was supported by research fund from the National Basic Research Program of China (973 Program, No. 2015CB251503) and the 111 Project (B12034).

Reference

- [1] Kim H, Ham J, Park C, Cho H. Theoretical investigation of the efficiency of a U-tube solar collector using various nanofluids. Energy, 2016, 94: 497-507.
- [2] Kim H, Kim J, Cho H. Experimental study on performance improvement of U-tube solar collector depending on nanoparticle size and concentration of Al₂O₃ nanofluid. Energy, 2016.
- [3] Al-Nimr MA, Al-Dafaie AMA. Using nanofluids in enhancing the performance of a novel two-layer solar pond. Energy, 2014, 68: 318-326.
- [4] Chen M, He Y, Zhu J, Wen D. Investigating the collector efficiency of silver nanofluids based direct absorption solar collectors. Applied Energy, 2016, 181: 65-74.

- [5] Kosuga A, Yamamoto Y, Miyai M, et al. A high performance photothermal film with spherical shell-type metallic nanocomposites for solar thermoelectric conversion. *Nanoscale*, 2015, 7(17): 7580-4.
- [6] Lenert A, Wang E N. Optimization of nanofluid volumetric receivers for solar thermal energy conversion. *Solar Energy*, 2012, 86(1): 253-265.
- [7] De Boni L, Wood E L, Toro C, et al. Optical Saturable Absorption in Gold Nanoparticles. *Plasmonics*, 2008, 3(4): 171-176.
- [8] Colangelo G, Favale E, Miglietta P, et al. Thermal conductivity, viscosity and stability of Al₂O₃-diathermic oil nanofluids for solar energy systems. *Energy*, 2016, 95: 124-136.
- [9] Tyagi H, Phelan P, Prasher R. Predicted Efficiency of a Low-Temperature Nanofluid-Based Direct Absorption Solar Collector. *Journal of Solar Energy Engineering*, 2009, 131(4): 041004.
- [10] Doak J, Gupta R K, Manivannan K, et al. Effect of particle size distributions on absorbance spectra of gold nanoparticles. *Physica E: Low-dimensional Systems and Nanostructures*, 2010, 42(5): 1605-1609.
- [11] Liu X, Atwater M, Wang J, et al. Extinction coefficient of gold nanoparticles with different sizes and different capping ligands. *Colloids Surf B Biointerfaces*, 2007, 58(1): 3-7.
- [12] Chen M, He Y, Zhu J, et al. Enhancement of photo-thermal conversion using gold nanofluids with different particle sizes. *Energy Conversion and Management*, 2016, 112: 21-30.
- [13] Mercatelli L, Sani E, Zaccanti G, et al. Absorption and scattering properties of carbon nanohorn-based nanofluids for direct sunlight absorbers. *Nanoscale Res Lett*, 2011, 6(1): 282.
- [14] Chen M, He Y, Zhu J, et al. An experimental investigation on sunlight absorption characteristics of silver nanofluids. *Solar Energy*, 2015, 115: 85-94.
- [15] Karami M, Akhavan-Behabadi M A, Raisee Dehkordi M, et al. Thermo-optical properties of copper oxide nanofluids for direct absorption of solar radiation. *Solar Energy Materials and Solar Cells*, 2016, 144: 136-142.
- [16] Lucas T M, Moiseeva E V, Zhang G, et al. Thermal properties of infrared absorbent gold nanoparticle coatings for MEMS applications. *Sensors and Actuators A: Physical*, 2013, 198: 81-86.
- [17] Kim J-H, Lavin B W, Boote B W, et al. Photothermally enhanced catalytic activity of partially aggregated gold nanoparticles. *Journal of Nanoparticle Research*, 2012, 14(7).
- [18] Nair R G, Tripathi A M, Samdarshi S K. Photocatalytic activity of predominantly rutile mixed phase Ag/TiV oxide nanoparticles under visible light irradiation. *Energy*, 2011, 36(5): 3342-3347.
- [19] El-Sayed IH, Huang X, El-Sayed MA. Selective laser photo-thermal therapy of epithelial carcinoma using anti-EGFR antibody conjugated gold nanoparticles. *Cancer Letters*, 2006, 239(1): 129-35.
- [20] Ou G, Li Z, Li D, et al. Photothermal therapy by using titanium oxide nanoparticles. *Nano Research*, 2016, 9(5): 1236-1243.
- [21] Ye S, Marston G, McLaughlan J R, et al. Engineering gold nanotubes with controlled length and near-Infrared absorption for theranostic applications. *Advanced Functional*

- Materials, 2015, 25(14): 2117-2127.
- [22] Liu H, Liu T, Wang H, et al. Impact of PEGylation on the biological effects and light heat conversion efficiency of gold nanoshells on silica nanorattles. *Biomaterials*, 2013, 34(28): 6967-75.
- [23] Bhana S, Lin G, Wang L, et al. Near-infrared-absorbing gold nanopopcorns with iron oxide cluster core for magnetically amplified photothermal and photodynamic cancer therapy. *ACS Applied Materials & Interfaces*, 2015, 7(21): 11637-47.
- [24] Zhou J, Wang Z, Li Q, Liu, F., Du, Y., Yuan, H., Hu, F., Wei, Y., You, J. Hybridized doxorubicin-Au nanospheres exhibit enhanced near-infrared surface plasmon absorption for photothermal therapy applications. *Nanoscale*, 2015, 7(13): 5869-83.
- [25] Paci B, Generosi A, Albertini V R, et al. Enhancement of photo/thermal stability of organic bulk heterojunction photovoltaic devices via gold nanoparticles doping of the active layer. *Nanoscale*, 2012, 4(23): 7452-9.
- [26] Ebrahimian M, Ansarifar G R. Investigation of the nano fluid effects on heat transfer characteristics in nuclear reactors with dual cooled annular fuel using CFD (Computational Fluid Dynamics) modeling. *Energy*, 2016, 98: 1-14.
- [27] Garoosi F, Hoseininejad F, Rashidi M M. Numerical study of natural convection heat transfer in a heat exchanger filled with nanofluids. *Energy*, 2016, 109: 664-678.
- [28] Lee J W, Kang Y T. CO₂ absorption enhancement by Al₂O₃ nanoparticles in NaCl aqueous solution. *Energy*, 2013, 53: 206-211.
- [29] Zhang H, Chen H-J, Du X, Wen D. Photothermal conversion characteristics of gold nanoparticle dispersions. *Solar Energy*, 2014, 100: 141-147.
- [30] Richardson H H, Carlson M T, Tandler P J, et al. Experimental and theoretical studies of light-to-heat conversion and collective heating effects in metal nanoparticle solutions. *Nano Lett*, 2009, 9(3): 1139-46.
- [31] Chen H J, Wen D. Ultrasonic-aided fabrication of gold nanofluids. *Nanoscale Res Lett*, 2011, 6(1): 198.
- [32] Philip D. Synthesis and spectroscopic characterization of gold nanoparticles. *Spectrochim Acta A Mol Biomol Spectrosc*, 2008, 71(1): 80-5.
- [33] Kim JH, Lavin BW. Preparation of gold nanoparticle aggregates and their photothermal heating property. *Journal of Nanoscience and Nanotechnology*, 2011, 11(1): 45-52.
- [34] Chen H J, Wen D. Ultrasonic-aided fabrication of gold nanofluids. *Nanoscale Research Letters*, 2011, 6(1):1-8(8).
- [35] Chen J, Wang D, Xi J, Au L, Siekkinen A, Warsen A, Li Z, Zhang H, Xia Y, Li X. Immuno gold nanocages with tailored optical properties for targeted photothermal destruction of cancer cells. *Nano letters*, 2007, 7(5):1318.
- [36] He, Q., Wang, S., Zeng, S, Zheng, Z. Experiemtnal investigation on photothermal properties of nanofluids for direct absorption solar thermal energy systems. *Energy Conversion and Management*, 2013, 73:150-157.
- [37] Jin, H., Lin, G., Bai, L., Amjad, M., Bandarra Filho, E.P., Wen, D. Photothermal conversion efficiency of nanofluids: An experimental and numerical study. *Solar Energy*, 2016, 139:278-289.

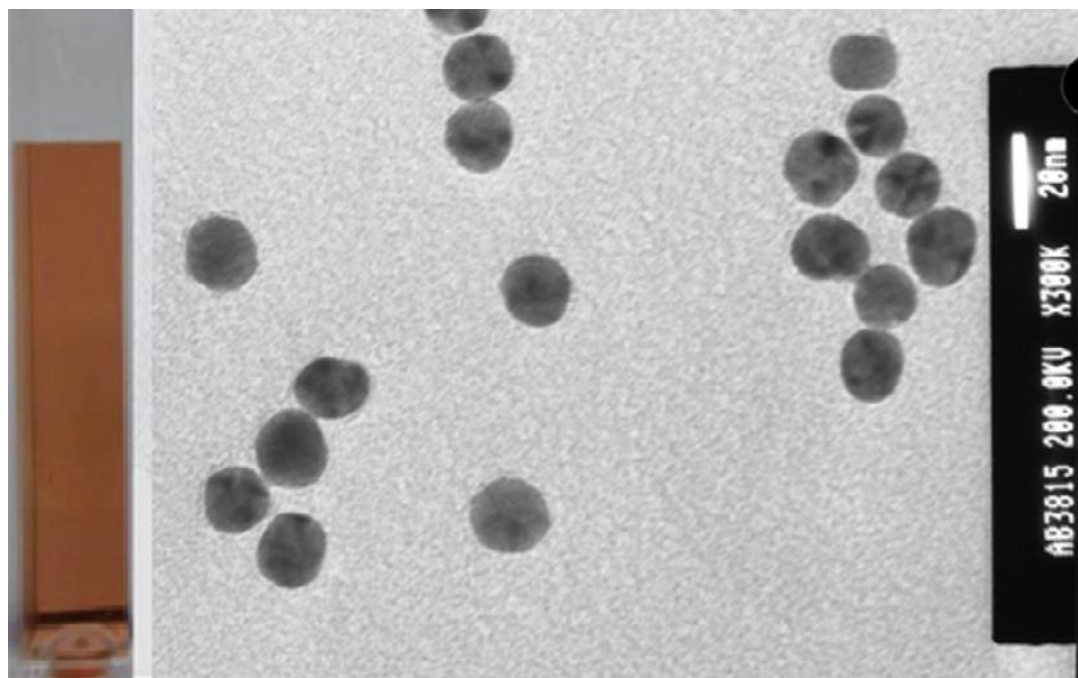


Fig. 1. TEM image of GNPs, inset: resulting dispersion of red-wine color.

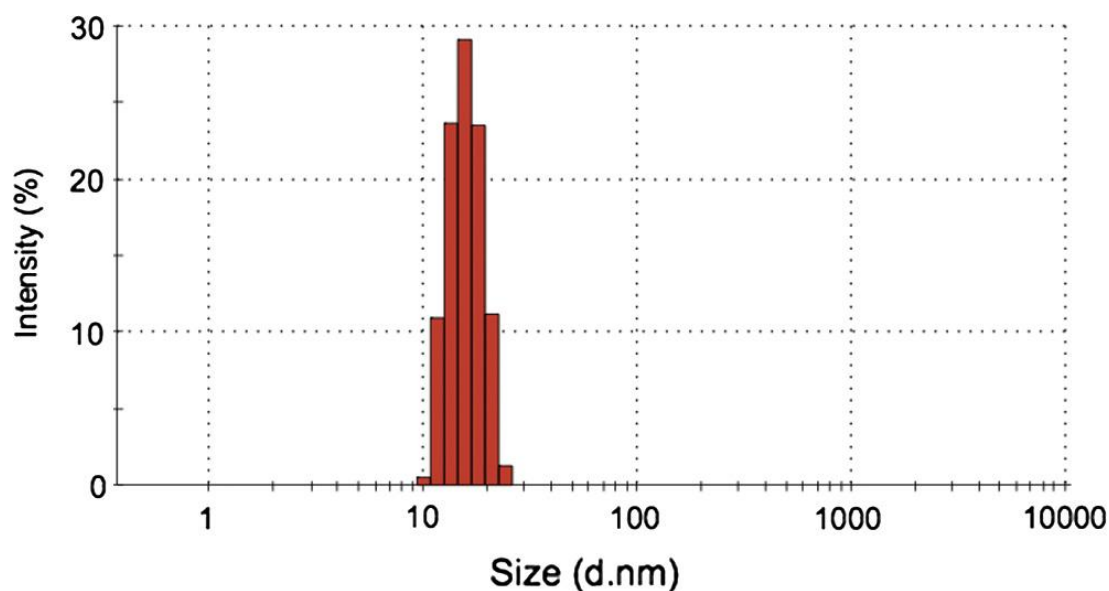


Fig. 2. Particle size distributions in an aqueous medium measured by dynamic light scattering (DLS) .

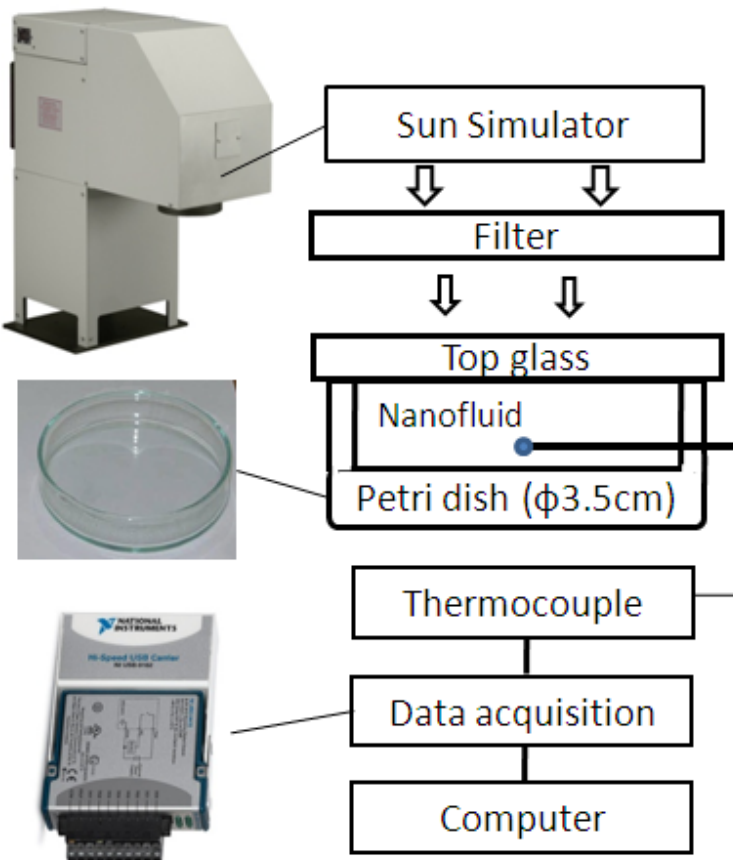


Fig. 3. Schematic illustration of the photothermal conversion experimental system.

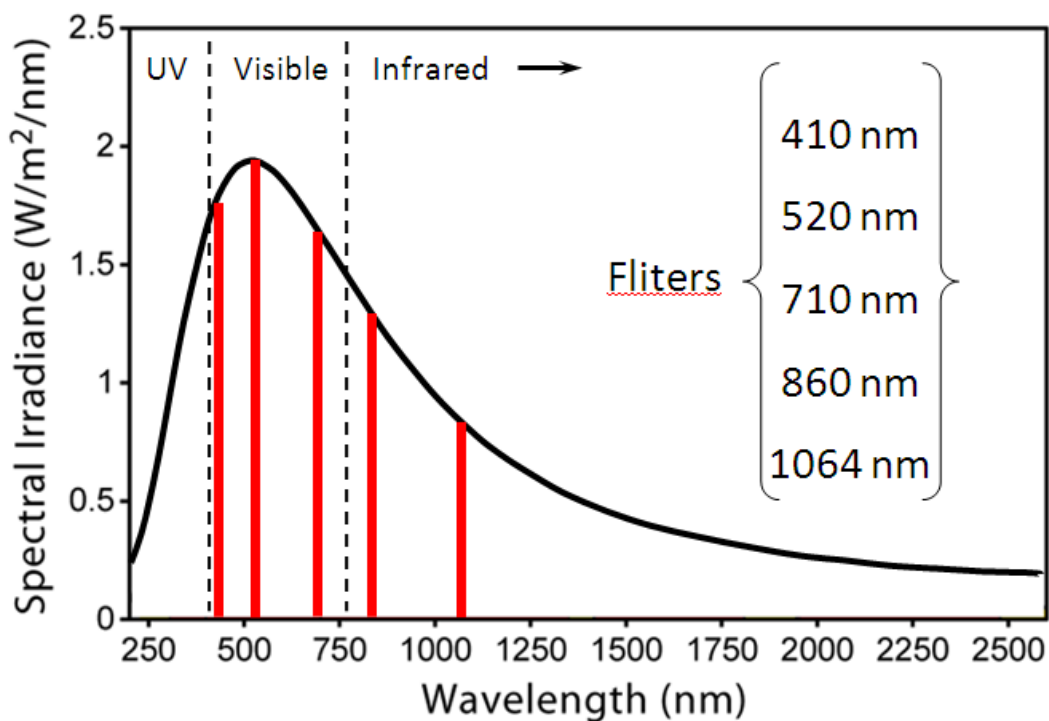
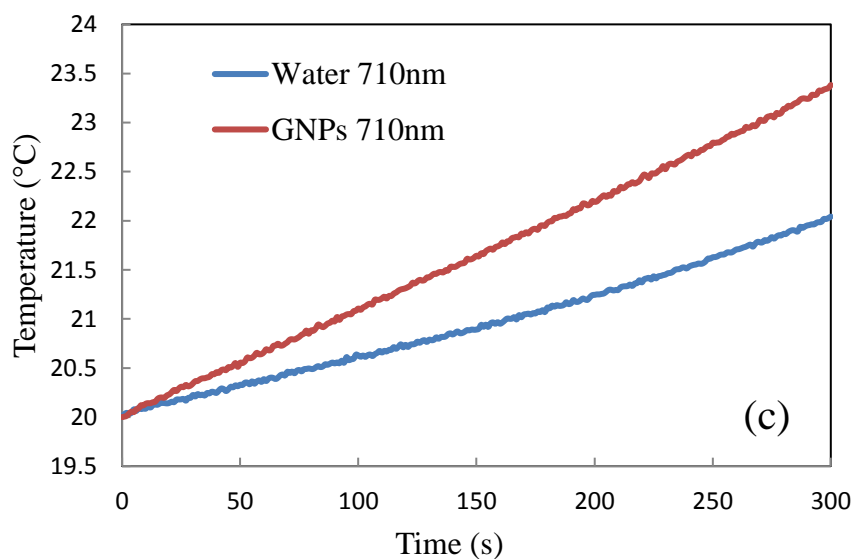
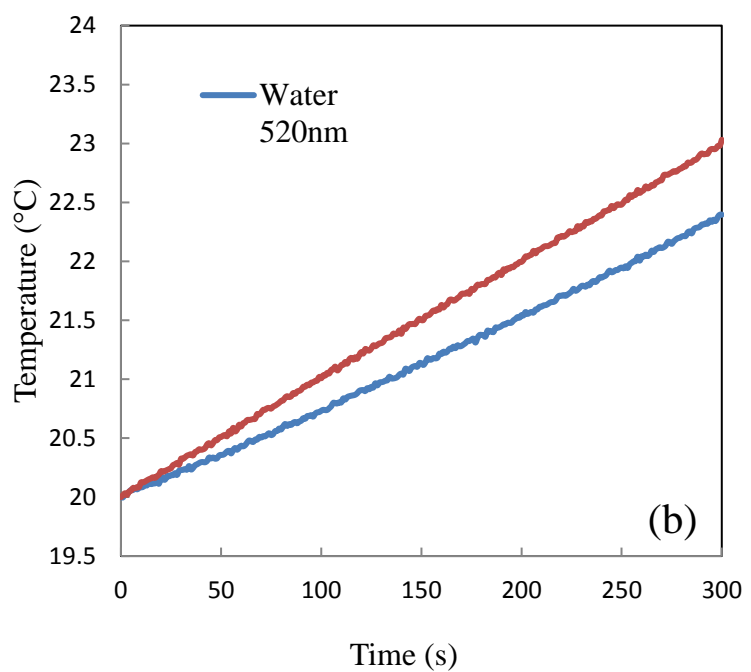
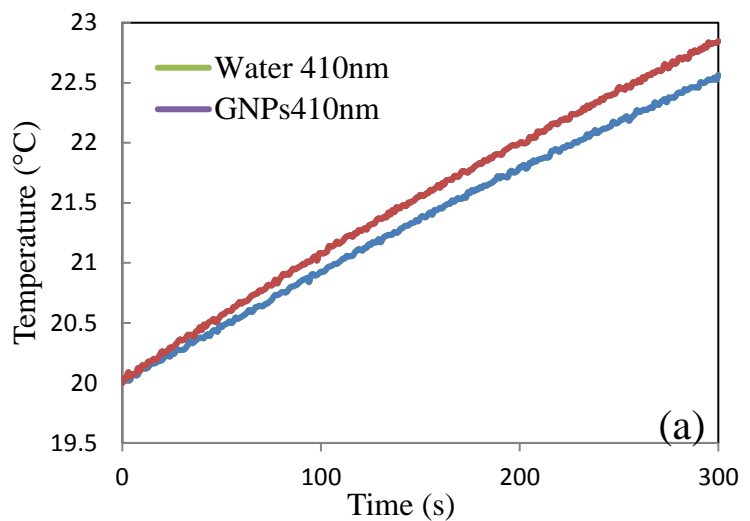


Fig. 4. Solar radiation spectrum and filters used in the experiment.



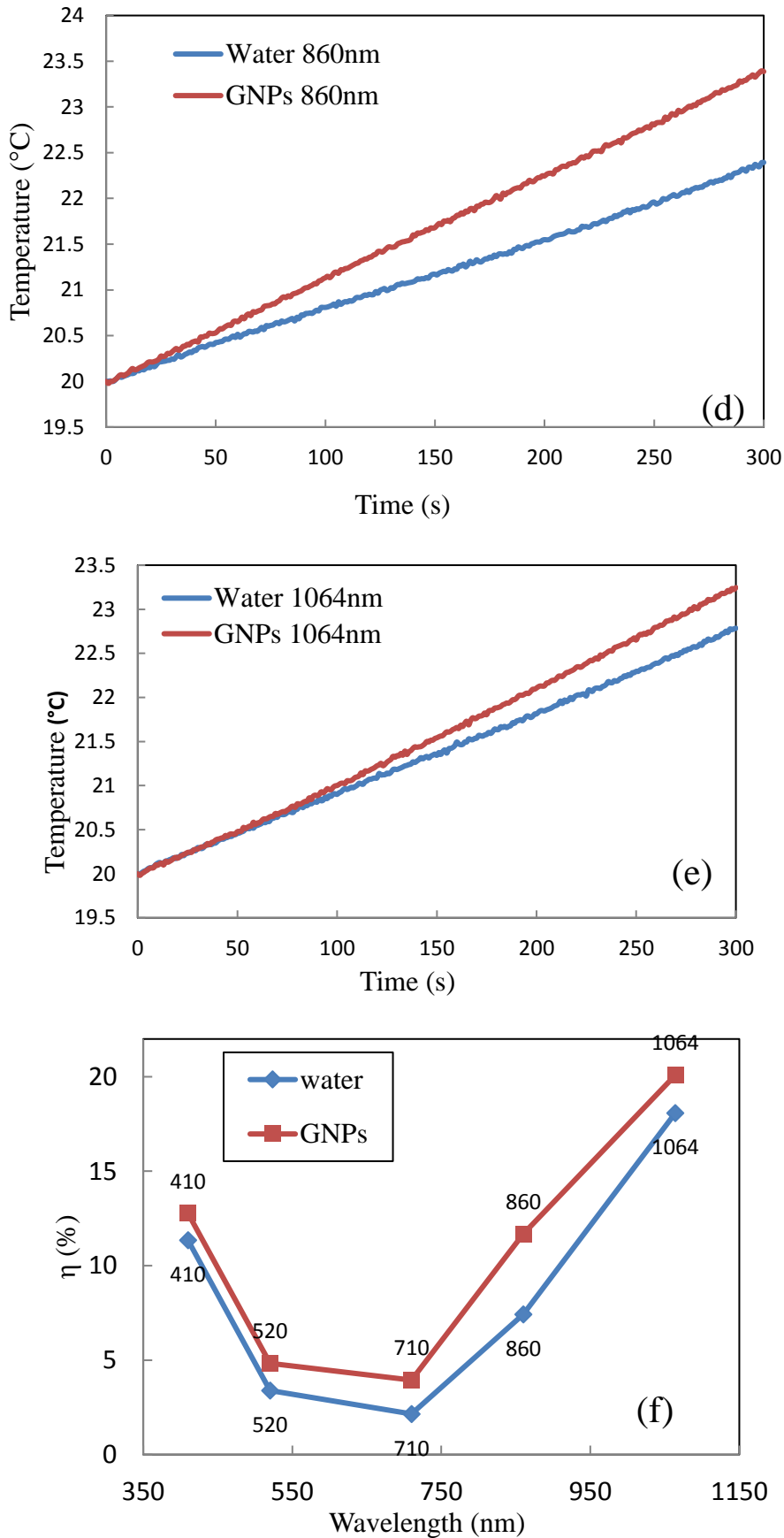


Fig. 5. Photothermal conversion efficiencies of GNPs at different filters conditions.

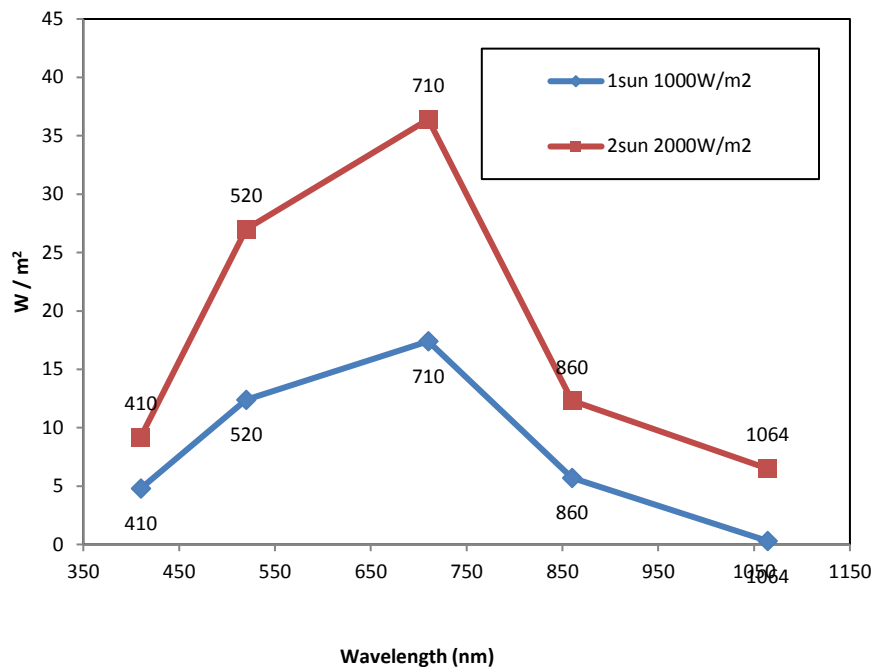


Fig. 6. Light intensities passing through filters.

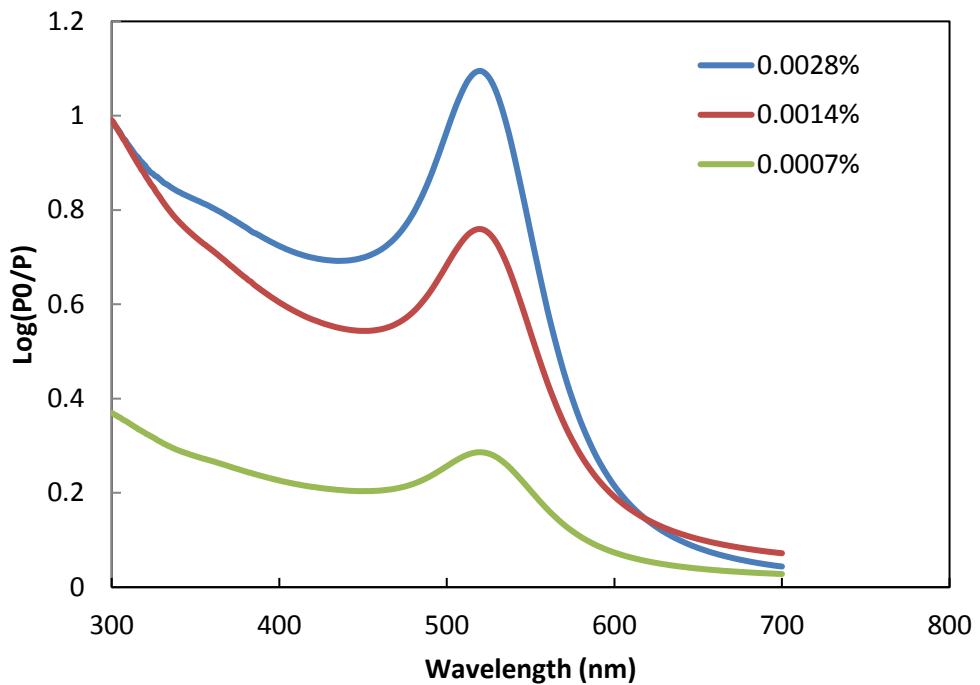


Fig. 7. The absorbance spectrum of gold nanofluids at different mass concentrations (extinction coefficient).

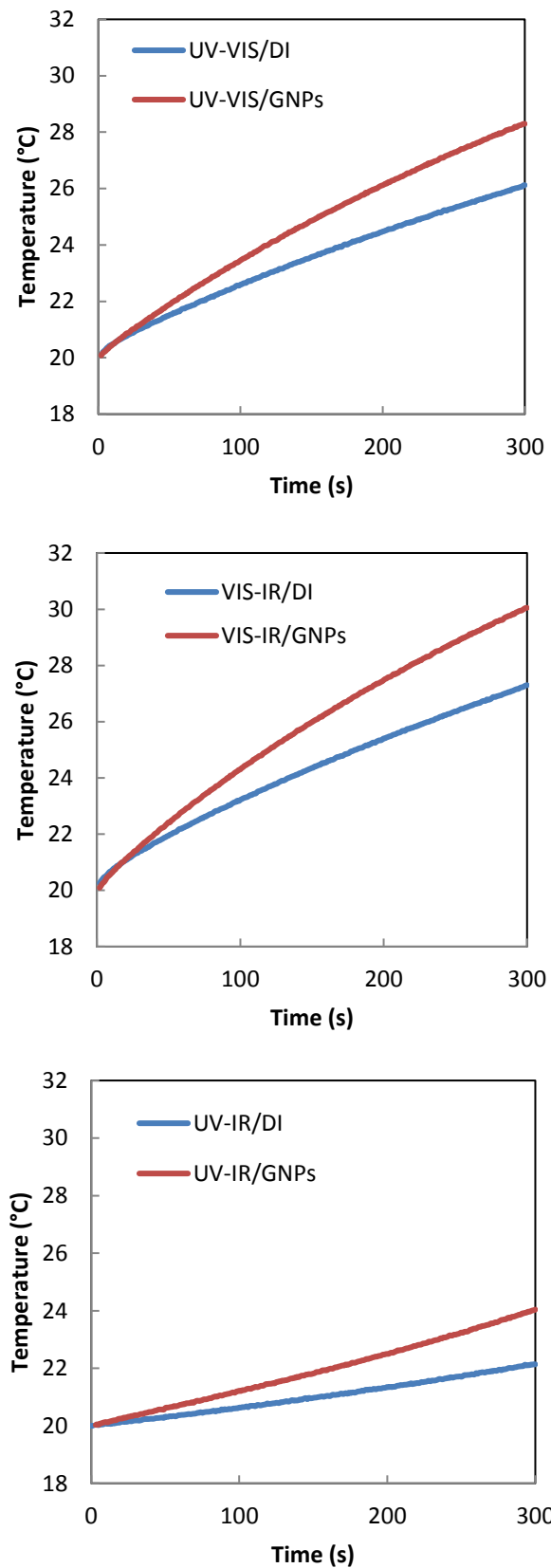


Fig. 8. The temperature lines in UV-VIS, UV-IR, VIS-IR waveband.

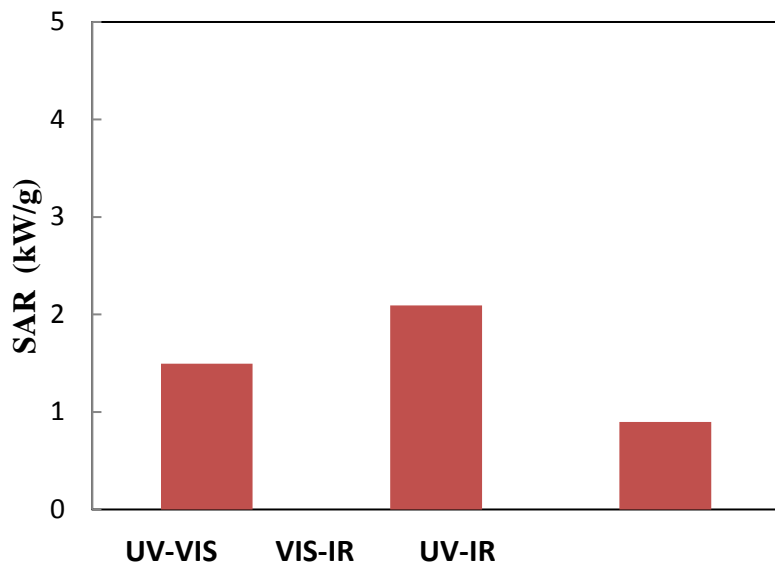


Fig. 9. UV-VIS, UV-IR, VIS-IR wavelength SAR of GNPs at AM = 1.5.

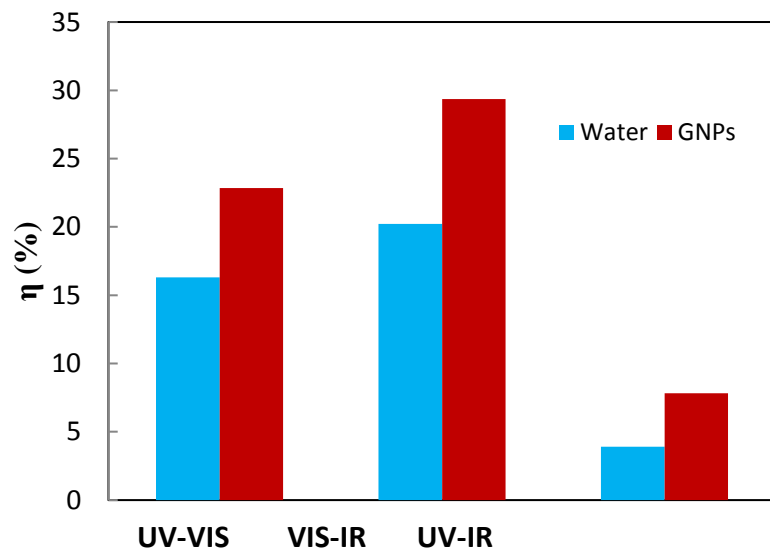


Fig. 10. Photothermal conversion efficiency (η) of GNPs and DI water in UV-VIS, UV-IR, VIS-IR waveband.